Hindawi
Wireless Communications and Mobile Computing
Volume 2018, Article ID 6795931, 17 pages
https://doi.org/10.1155/2018/6795931

Research Article

Empirical Path-Loss Modeling and a RF Detection Scheme for Various Drones

Won Ho Jeong,[1] **Hong-Rak Choi**,[2] **and Kyung-Seok Kim**[2]

[1]*Convergence Technology Team, Department of Business Support, Gyeongbuk Institute of IT Convergence Industry Technology, Gyeongsan, Gyeongbuk, Republic of Korea*
[2]*The Smart Radio Communication System Lab., Department of Radio & Communication Engineering, Chungbuk National University, Cheongju, Chungbuk, Republic of Korea*

Correspondence should be addressed to Kyung-Seok Kim; kseokkim@cbnu.ac.kr

Received 13 July 2018; Accepted 14 November 2018; Published 6 December 2018

Academic Editor: Maode Ma

This paper presents a path-loss model based on a radio-frequency (RF) detection scheme for various drones using 5G aerial communication over an industrial, scientific, and medical radio band (ISM band) network. We considered three communication modes of the ISM band for the channel characteristics analysis: the DJI Enhanced Spread Spectrum Technology (DESST) protocol, Wi-Fi, and Bluetooth. The drone signal detection scheme extracts the drone signal from the environment mixed with the general signal. The drone DESST signal is identified through cross-correlation of the received signal. The Wi-Fi and Bluetooth signals are identified with the singular-value decomposition (SVD) algorithm by using the hopping characteristics. General and drone Wi-Fi signals are separated by in-phase/quadrature (I/Q) phase analysis over the measurement time. The windowed received signal strength indicator (RSSI) moving detection (WRMD) analysis identifies the drone Bluetooth signal according to the movement of the drone. The detected drone signal is channel modeled by the horizontal distance d according to the altitude θ. Finally, they verify their model by a ray-tracing simulation similar to the real environment. The model provides a simple and accurate prediction for designing future aerial communications systems according to changes in drone movement.

1. Introduction

Drones refer to unmanned aerial vehicles (UAVs) that can be controlled by radio waves, which means that an aircraft can fly remotely or automatically without a person on board. Although drones were originally developed for military use, they are rapidly spreading into the industrial and civilian markets as they become more widely used in various fields. The Till Group, a US consulting firm, predicted that the world market for drones would surge by more than four times from 2.8 billion dollars in 2017 to 11.8 billion dollars in 2026. In recent years, global companies such as DJI (Da Jiang Innovation), Amazon, and Google have participated in the development of drones, and their value is increasing in various fields. The applications for drones are numerous, ranging from package delivery, aerial photography, agriculture and pest control, site inspection, and surveys to public safety services such as providing coverage for remote areas [1, 2].

As the field of these applications increases, the abuse of drones is increasing. Drones are difficult to recognize and defend against because they can be accessed from a distance by radio waves. In 2015, a cesium drone was found on the roof of the prime minister's house in Japan and in 2017, there was an unmanned landing in Korea. Drone detection methods include RF detection, radar detection, infrared detection, image detection, and voice detection. When constructing a drone defense system, more than 90% of drone detection technology relies on RF detection and physical detection of radar, and complex sensing is performed after the RF detection alarm. This RF detection technique has a disadvantage in that the accuracy is low when other signals exist in the same frequency band. Therefore, in this paper, we describe a drone RF detection technique where there is a general terminal signal in the same frequency band.

Currently, a method that uses a short range wireless communication network, a 4G/5G mobile communication

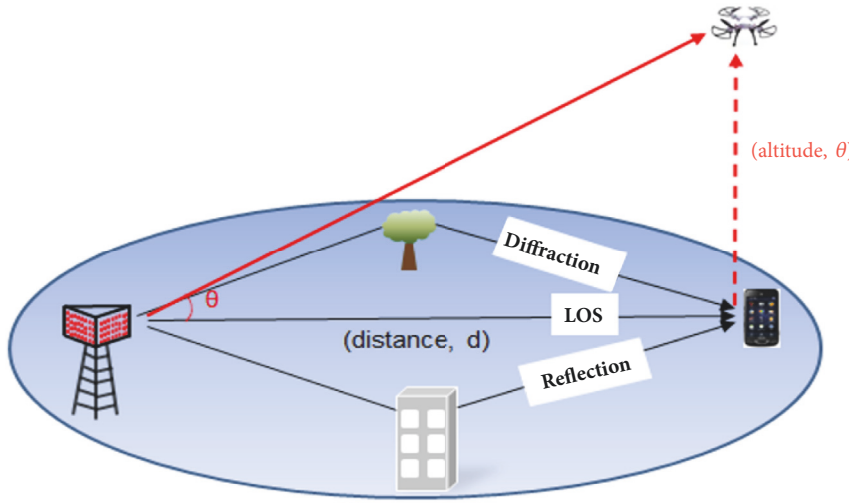

Figure 1: Proposed path-loss model for the ISM band drone system.

network, and a satellite GPS network as a drone wireless communication method exists. When the mobile communication network and the GPS network are used, there is a problem regarding frequency use permission and data-base transmission, and at present, more than 90% of commercial drones use the short range wireless communication network. Therefore, the RF detection and path loss modeling of this paper focus on the short range wireless communication network. First, RF detection of drones using Wi-Fi, DESST (DJI Enhanced Spread Spectrum Technology), and Bluetooth protocol is performed among typical communication methods of local wireless communication networks. The frequency band is measured in the 2.4 GHz band for the small drones, according to the distribution status of the WRC-15 domestic drone frequency, and the results are derived [3]. This frequency band is the 1218 drones used in the 2018 PyeongChang Winter Olympics. For this ceremony, it is necessary to distinguish the band from the general Wi-Fi and Bluetooth signals used by tens of thousands of people, preventing entry of other drone signals. In the 2.4 GHz band, the signal identified according to the proposed RF detection scheme carries out path loss modeling according to three protocols. Drone communications focus on 3GPP standardization activities and on connectivity service requirements for evaluation scenarios and channel models [4]. 3D channel modeling is based on the straight line distance, according to distance and altitude, and does not accurately reflect path loss due to altitude. The modeling work in [5–13] suggests that the altitude loss of a UAV is similar to the free space propagation model. The authors point out the need for height-dependent parameters for describing the propagation channel of UAVs. In this paper, we propose a new modeling approach for the suburban communication channel, capable of capturing the mean path-loss between a drone channels characterization and endured shadowing statistics. We characterize the path-loss as an excess value added to the already-known standard path-loss. This excess has a strong dependence on the depression angle as proven by the experimental results. The proposed model is validated by comparing with existing model through a ray-tracing simulation.

This paper is organized as follows. Section 2 introduces the flow of our proposed model. Section 3 introduces the measurement system and measurement scenarios at Chungbuk National University. Section 4 presents radio-frequency (RF) detection schemes for various drone classifications. Section 5 presents the proposed path-loss models for various drones. Section 6 proposes the path-loss models and verifies our model through the ray-tracing simulation. Finally, Section 7 provides concluding remarks and summarizes this paper.

2. Flow of the Proposed Path-Loss Model

We propose a channel model for distance d and altitude θ and performed field tests for three kinds of drones in the industrial, scientific, and medical radio band (ISM band) at 2.4 GHz. The standard 3GPP spatial channel model was created by simplifying the COST 231 or WINNER II channel model [14, 15]. This channel model is based on geometric stochastic channel modeling and shows diffraction, reflection, or shadowing with a straight distance d at an antenna maximum height of 25 m. This standard model describes the path loss for the distance d in various scenarios but does not account for the path loss i according to the drone altitude. Therefore, we propose a path-loss model based on the drone flight by channel modeling with the horizontal distance d and altitude θ, as shown in Figure 1.

The proposed path-loss modeling process is as shown in Figure 2. First, the measurement results are used to identify the drone signal excluding the general terminal signal based on the RF identification algorithm described in Section 4. For drones using the DJI Enhanced Spread Spectrum Technology

Table 1: Specifications of measurement drones.

Parameters	DESST (DJI MAVIC PRO)	Wi-Fi (K2-02)	Bluetooth (Airborne Night)
Size	45 × 45 cm (Micro-drone)	50 × 50 cm (Micro-drone)	15 × 15 cm (Nano-drone)
Max. flight time	23 min.	8 min.	7 min
Max. flight speed	40 m/s	20 m/s	5 m/s
Frequency band		2.4–2.5 GHz	

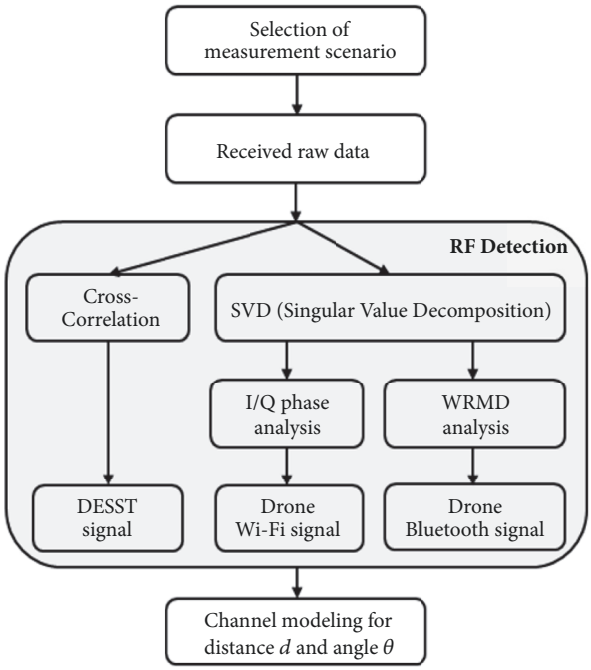

Figure 2: Procedure of the proposed model.

(DESST) protocol, the cross-correlation algorithm is applied to identify the drone signal. The singular-value decomposition (SVD) algorithm is applied to distinguish the next hopping Bluetooth signal from a Wi-Fi signal using a fixed channel. The drone Wi-Fi signal is then identified through in-phase/quadrature (I/Q) phase analysis to distinguish the Wi-Fi signal from the dongle Wi-Fi signal. Finally, the drone Bluetooth signal is identified with the windowed received signal strength indicator (RSSI) moving detection (WRMD) method. The identification signals for the three drones are obtained from each scenario and modeled according to the horizontal distance and altitude. The model equation is derived by fitting the measurement results according to the distance, and the power values derived at intervals of 10 m are subtracted from the measured data values for the altitude path-loss modeling. The loss values according to the altitude are analyzed according to the distances. The path-loss model equation according to the final altitude is derived by fitting the loss value according to the altitude.

3. Measurement Setup

For path-loss modeling, we constructed a measurement system and used DESST, Wi-Fi, and Bluetooth drones. The communication of general terminals is freely used in Wi-Fi and Bluetooth protocols, but drone communication is limited due to Korean drone flight regulations. Therefore, after the approval of the government, the measurement was carried out at Chungbuk National University. The measurement area has been selected according to the ITU-R environmental classification for urban, suburban, and rural environments [16, 17]. The measurement environments reflect surrounding trees, bushes, buildings, and vehicle movement information. It shows the propagation environment of the drone mixed with general terminal signals well. We measured a total of three sites and obtained 15000-70000 data samples and averaged over 8 repeated measurements at each site. Figure 3 shows a satellite photograph of the measurement area. The spectrum analyzer (RSA-306) used for measurement was located 1.5 m from the end of the ground.

3.1. Measurement System. The RSA-306 (Tektronix) spectrum analyzer was used for measurement. The RSA-306 is a handheld device that can be powered and connected via USB 3.0. It has a measurable frequency range of 9 kHz–6.2 GHz and is capable of measuring the 2.4 GHz band of the ISM band with a measurement bandwidth of 40 MHz. The dynamic range is −160 dBm to 23 dBm. The RSA-306 can be connected with the MATLAB software for real-time signal processing of the received data. The first received signal is received as I / Q data; it is analyzed in power spectrum and spectrogram form by signal processing. The drones used DESST, Wi-Fi, and Bluetooth in the ISM band. Figure 4 shows the three drones and Table 1 presents their specifications.

3.2. Measurement Scenarios. As shown in Figure 5, scenario 1 was to derive the path-loss equation according to the distance. The general Wi-Fi and Bluetooth signals were fixed 3 m away from each other, and the dedicated drone was moved 5–70 m in the straight direction. As shown in Figure 6, scenario 2 was to perform a moving measurement 1.5–101.5 m above a point at intervals of 10 m and a speed of 4 m/s. Table 2 presents the measured bandwidth of 40 MHz at a carrier frequency of 2.45 GHz. The noise power of the spectrum analyzer was −134 dBm/Hz. In Korea's 2.4GHz band, more than 90% of the drones use DESST, Wi-Fi, and Bluetooth protocols. Further,

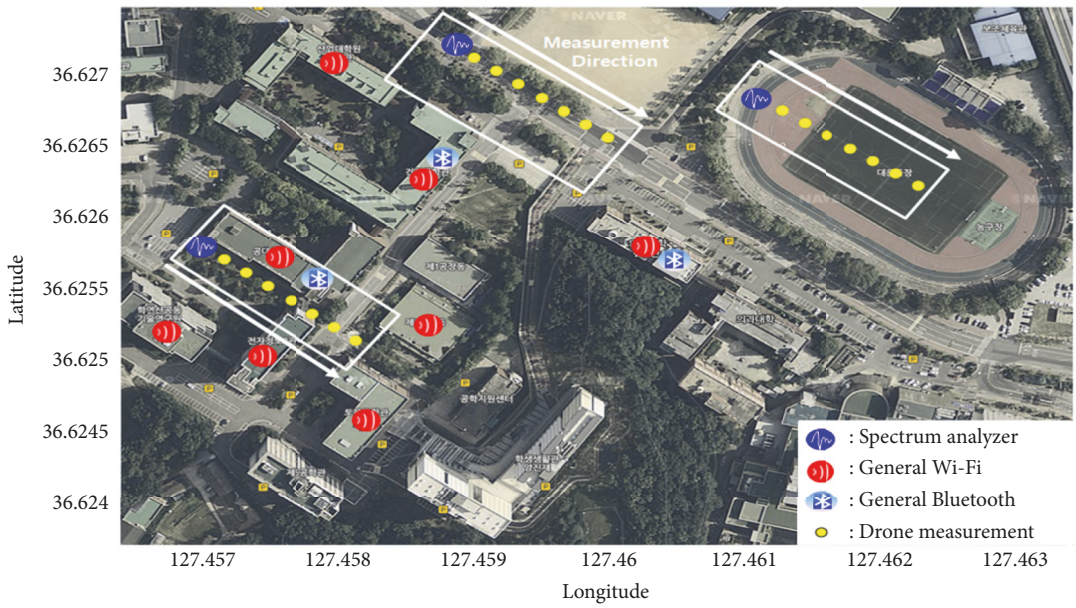

Figure 3: Satellite photograph of the measurement area.

(a) (b) (c)

Figure 4: Measurement drones: (a) DJI MAVIC PRO, (b) K2-02, and (c) Airborne Night.

Korean commercial drones market is dominated by DJI in China and PARROT in France [18]. Therefore, DJD MAVIC PRO of DJI and Airborne Night of PARROT were used as measurement drones. Because of the difficulty of radio certification, the Wi-Fi drones were measured using K2-02 of Kid's World, which has been certified by Korean radio communications.

4. Radio-Frequency Detection Schemes for Drone Classification

All field measurements were based on the scenarios presented in Section 3. The drone identification process was performed using the signal processing flowchart shown in Figure 7. The drone signals using different communication methods were identified step by step, and each signal was distinguished by repeating the measurements.

Although the identification results were distinguished by the measurement scenario, the DESST drone, general Wi-Fi, Wi-Fi drone, general Bluetooth, and Bluetooth drone signals can be rewritten as follows:

$$Y(t) = y_{D\_DESST}(t) + y_{D\_WF}(t) + y_{WF}(t) + \ldots y_{D\_BT}(t) + y_{BT}(t) + n_0 \quad (1)$$

where Y is all received signals at the measurement time, y_{D_DESST} is the DESST drone signal, y_{D_WF} is the drone Wi-Fi signal, y_{WF} is the general Wi-Fi signal, y_{D_BT} is the drone Bluetooth signal, y_{BT} is the general Bluetooth signal, n_0 is the zero-mean Gaussian noise, and t is the measurement time.

Table 2: Measurement setup parameters.

Parameters	Value
Carrier frequency	2.45 GHz
Bandwidth	40 MHz
Study area	100 m^2
Mean aerial speed	4 m/s
Spectrum analyzer height	1.5 m
Measurement radius	10–70 m (step: 10 m)
Measurement altitude	1.5–101.5 m
Noise power density	−134 dBm/Hz

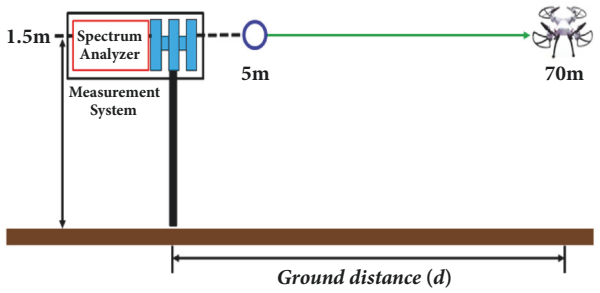

Figure 5: Measurement scenario 1 (5–70 m horizontal movement).

In the proposed scheme, the drone signal is distinguished according to each signal's characteristic.

4.1. Cross-Correlation for DESST Drone Detection. For signal identification, the normal Wi-Fi and Bluetooth signals are measured simultaneously. The dedicated drone signal repeats channel hopping and fixing according to the measurement time, has a bandwidth of 1–2 MHz, and takes the shape of a square wave. By using the characteristics of this signal, any square wave with a bandwidth of 1–2 MHz can be generated to identify the signal through the cross-correlation scheme. The generated square wave signal can be rewritten as

$$v(t) = \begin{cases} 1, & DESST\_protocol \\ 0, & otherwise \end{cases} \quad (2)$$

The generated square wave signal is cross-correlated as follows:

$$\rho(x, y) = \frac{\sum_{i=1}^{N} (x(i) - \overline{x})(y(i) - \overline{y})}{\sqrt{\sum_{i=1}^{N} (x(i) - \overline{x})^2 \sum_{i=1}^{N} (y(i) - \overline{y})^2}} \quad (3)$$

where x is the generated square wave signal and y is all other measured signals. Table 3 presents the cross-correlation values of the measurement results for 20 s.

The analysis results confirmed that the dedicated drone signal had a high value. Therefore, if the cross-correlation value is over the threshold of 0.75, it is identified as a dedicated drone signal. The dedicated final drill identification formula is given as follows:

Table 3: Cross-correlation values for each signal.

	DESST	General Wi-Fi	General Bluetooth
Cross-correlation value	0.961	0.012	0.577

$$Y(t) = \begin{cases} y_{D\_DESST}, & \rho(t) > \rho_{D\_threshold} \\ y_{other\_sig}, & \rho(t) \le \rho_{D\_threshold} \end{cases} \quad (4)$$

The dedicated drone signal (i.e., DESST) is identified through a cross-correlation scheme because drone communication uses a proprietary protocol. Other signals can be identified through the SVD scheme regardless of whether they are drone or general signals, and then they can be evaluated as being a drone signal or general signal.

4.2. Singular Value Decomposition for Hopping Signal Detection. The remaining ISM band signals are divided into Wi-Fi and Bluetooth signals. Wi-Fi signals are measured by using the 802.11b communication standard, which is for both drones and general signals. The modulation uses the Gaussian frequency shift keying (GFSK) scheme and has a bandwidth of 20 MHz with 14 channels. The diffusion modulation method uses direct-sequence spread spectrum (DSSS) modulation and a fixed channel. Bluetooth uses the 802.15.1 communication standard and has a bandwidth of 1 MHz with 79 channels. In this case, the spreading modulation method is used by hopping the channel with the frequency-hopping spread spectrum (FHSS) for 625 μs [19]. The Wi-Fi communication standard uses one fixed channel. With the Bluetooth communication standard, the signal is randomly occupied for a predetermined time by avoiding the occupied channel without occupying a certain channel through hopping. We used this signal characteristic to identify the signals through the SVD scheme, which requires signals to be accumulated. The signal accumulation is given by

$$\overline{Y}(t_k) = \begin{bmatrix} Y(1) \\ Y(2) \\ \vdots \\ Y(k) \end{bmatrix},$$

$$\overline{y}_{D\_WF}(t_k) = \begin{bmatrix} y_{D\_WF}(1) \\ y_{D\_WF}(2) \\ \vdots \\ y_{D\_WF}(k) \end{bmatrix},$$

$$\overline{y}_{WF}(t_k) = \begin{bmatrix} y_{WF}(1) \\ y_{2,WF}(2) \\ \vdots \\ y_{k,WF}(k) \end{bmatrix}, \ldots$$

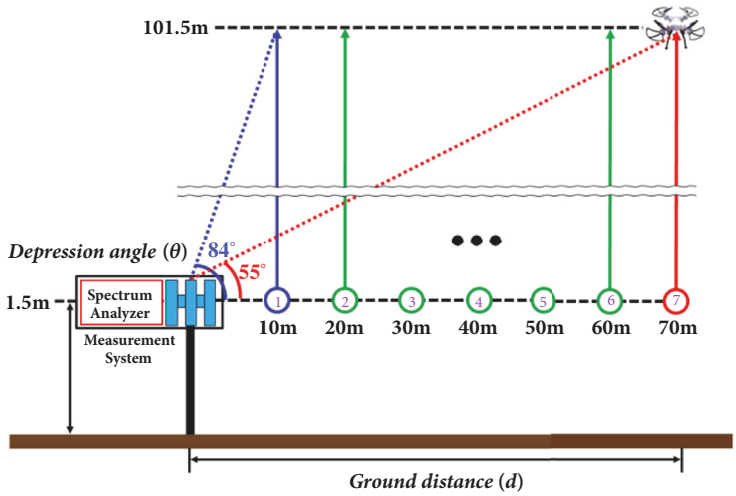

Figure 6: Measurement scenario 2 (horizontal: 10–70 m fixed (step: 10 m), altitude: 1.5–101.5 m (moving)).

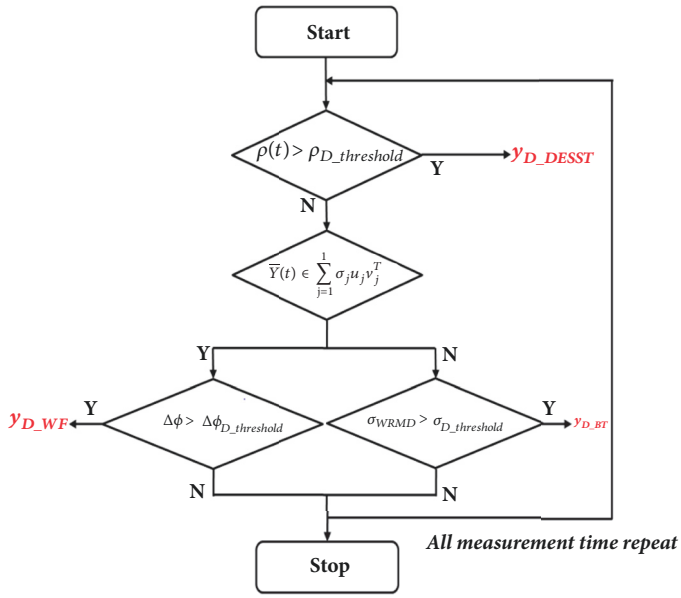

Figure 7: Flowchart for classifying the various drones.

$$\overline{y}_{D\_BT}(t_k) = \begin{bmatrix} y_{D\_BT}(1) \\ y_{D\_BT}(2) \\ \vdots \\ y_{D\_BT}(k) \end{bmatrix},$$

$$\overline{y}_{BT}(t_k) = \begin{bmatrix} y_{BT}(1) \\ y_{BT}(2) \\ \vdots \\ y_{BT}(k) \end{bmatrix} \tag{5}$$

The signals scaled by k times are decomposed by the following eigenvector decomposition:

$$\begin{aligned} \overline{Y}(t_k) &= USV^T \\ &= \begin{bmatrix} u_1 & u_2 & u_3 & \cdots & u_r \end{bmatrix} \begin{bmatrix} \sigma_1 & 0 & \cdots & 0 & 0 & \cdots & 0 \\ 0 & \sigma_2 & & \vdots & \vdots & & \vdots \\ \vdots & & \ddots & 0 & & & \\ 0 & 0 & \cdots & \sigma_r & 0 & \cdots & 0 \end{bmatrix} \begin{bmatrix} v_1^T \\ v_2^T \\ \vdots \\ v_r^T \end{bmatrix} \\ &= \sigma_1 \begin{pmatrix} \vdots \\ u_1 \\ \vdots \end{pmatrix} \begin{pmatrix} \cdots & v_1^T & \cdots \end{pmatrix} + \sigma_2 \begin{pmatrix} \vdots \\ u_2 \\ \vdots \end{pmatrix} \begin{pmatrix} \cdots & v_2^T & \cdots \end{pmatrix} \\ &\quad + \cdots + \sigma_r \begin{pmatrix} \vdots \\ u_r \\ \vdots \end{pmatrix} \begin{pmatrix} \cdots & v_r^T & \cdots \end{pmatrix} = \sum_{j=1}^{r} \sigma_j u_j v_j^T \end{aligned} \tag{6}$$

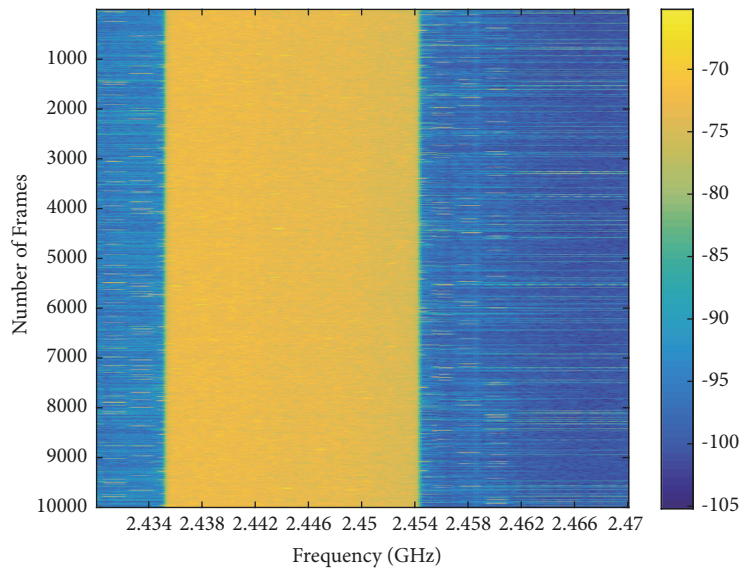

Figure 8: Spectrogram of the Wi-Fi and Bluetooth signals **before** the SVD scheme was applied.

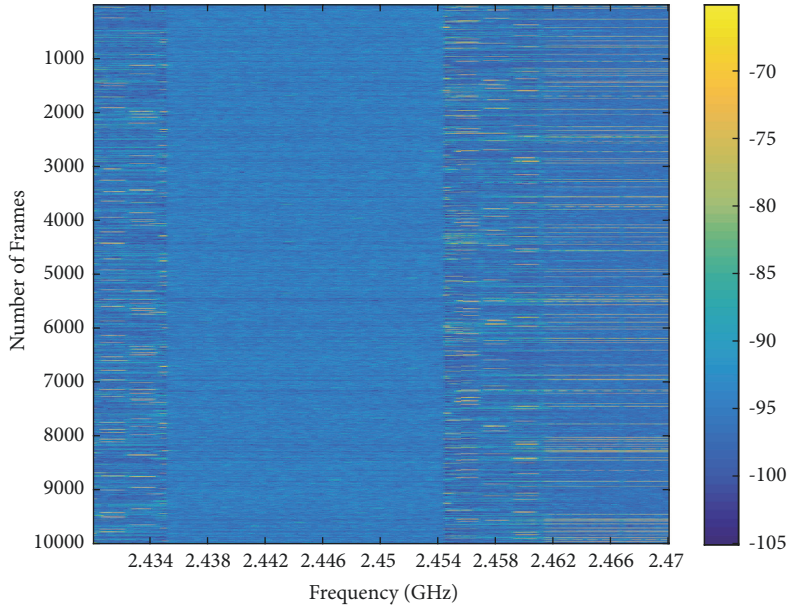

Figure 9: Spectrogram of the Bluetooth signal **after** the SVD scheme was applied.

where u_j is the left eigenvector, v_j^T is the right eigenvector, and σ_j is the singular value. The Wi-Fi signals that are fixed with one channel are subjected to eigenvector decomposition, so the eigenvalues of the signals are located at the top of the matrix. The eigenvalues of the Bluetooth signals hopping the channel are located in the remaining matrices. SVD is applied to signal identification as follows:

$$Y(t_k) = \begin{cases} y_{WF}(t_k) + y_{D\_WF}(t_k), & \overline{Y}(t_k) \in \sum_{j=1}^{1} \sigma_j u_j v_j^T \\ y_{BT}(t_k) + y_{D\_BT}(t_k), & \overline{Y}(t_k) \notin \sum_{j=1}^{1} \sigma_j u_j v_j^T \end{cases} \quad (7)$$

The values at the top of the SVD scheme are identified as the Wi-Fi signal, and the remainder is Bluetooth signals. Figures 8 and 9 are spectrogram graphs showing the measured drone, Wi-Fi, and Bluetooth signals accumulated by frequency before and after the SVD scheme was applied.

4.3. I/Q Phase Analysis for Wi-Fi Drone Detection. The signals identified by the SVD scheme are further identified as drone or general signals. The fixed channels of the Wi-Fi signals are identified by I/Q phase analysis. Drones generate Doppler frequencies as they fly, which affect the phasing of I/Q data. The electrical signals i and q before being processed with the power signal can be written as [20]

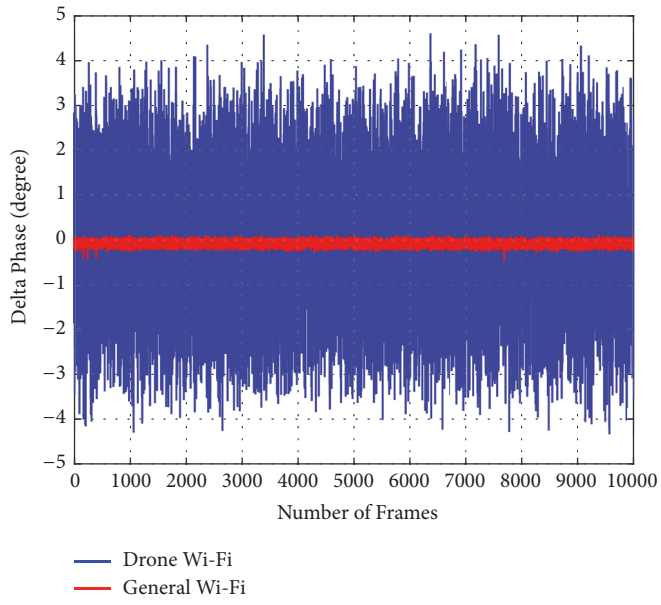

Figure 10: Difference in the I/Q phase according to time.

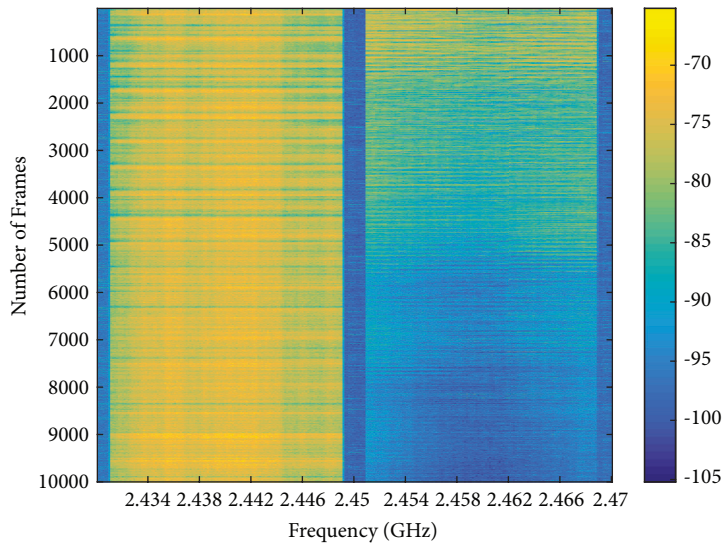

Figure 11: Spectrogram of the Wi-Fi signal **before** the I/Q phase analysis was applied.

$$Y(t) = I(t) + jQ(t) \tag{8}$$

The phase equation for drone signal identification can be written as

$$\Delta\phi = \tan^{-1}\left(\frac{Q(t)}{I(t)}\right) - \tan^{-1}\left(\frac{Q(t-1)}{I(t-1)}\right) \tag{9}$$

The frequency band signal located at the highest power value in the 20 MHz bandwidth is distinguished as being from a drone or not based on the phase difference with the previous signal. If the I/Q phase difference is above a certain value, the signal is identified as being a drone, and it is identified as a general signal if below.

$$Y(t) = \begin{cases} y_{D\_WF}(t), & \Delta\phi > \Delta\phi_{D\_threshold} \\ y_{WF}(t), & \Delta\phi < \Delta\phi_{D\_threshold} \end{cases} \tag{10}$$

Figure 10 shows the I/Q phase difference between the drone and general signals over time, and Table 4 presents the average value. Therefore, if the difference is 0.15 or more, the Wi-Fi signal is from a drone; if less, it is a general Wi-Fi signal. Figures 11 and 12 show spectrogram of the Wi-Fi signal before and after the I/Q phase analysis was applied.

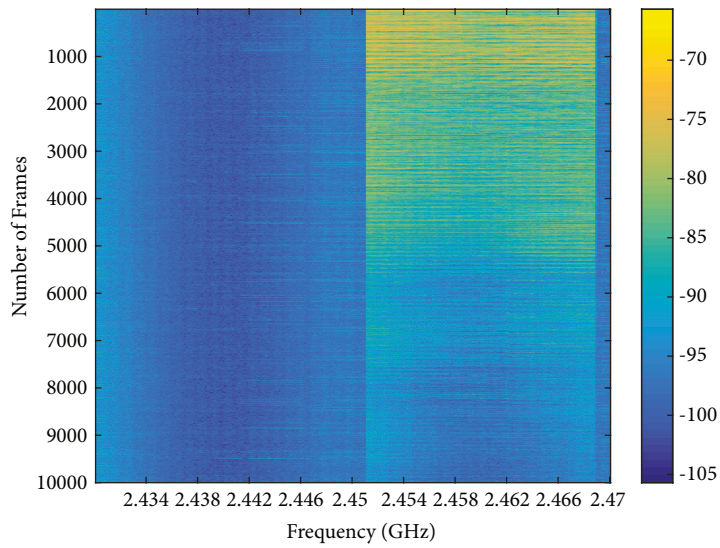

Figure 12: Spectrogram of the Wi-Fi signal **after** the I/Q phase analysis was applied.

Table 4: Average I/Q phase difference.

	Drone Wi-Fi	General Wi-Fi
I/Q phase difference value	0.2866	0.0317

4.4. Windowed RSSI Moving Detection for Bluetooth Drone Detection. The Bluetooth signal identified by the SVD scheme is further distinguished as a drone signal or general signal by the WRMD scheme. A flying drone moves at a higher speed than general Bluetooth signals. The WRMD scheme for calculating the power variation can be written as [21]

$$\sigma_{WRMD} = \sqrt{\frac{1}{K}\sum_{j=1}^{K}\left(Y_j(t) - \overline{Y}_m(t)\right)^2}, \quad m = n+1 \tag{11}$$

where n is the number of the WRMD window size. The signal is identified according to a threshold value:

$$Y(t) = \begin{cases} y_{D\_BT}(t), & \sigma_{WRMD} > \sigma_{D\_threshold} \\ y_{BT}(t), & \sigma_{WRMD} < \sigma_{D\_threshold} \end{cases} \tag{12}$$

WRMD is only applied when there is a difference of more than 5 dB between two or more extracted Bluetooth signals. This is based on the assumption that the drone is faster than the normal signal. Figure 13 shows a graph of the variation in the WRMD amplitude. Figures 14 and 15 show spectrograms of the Bluetooth signals before and after the WRMD scheme was applied.

5. Path-Loss Model for Three Standard Types

The identified drone signals are used to derive the channel model equation according to each distance d and altitude θ in the ISM band. The model equation was derived by first fitting the measurement results according to the distance, and the power value derived at intervals of 10 m was subtracted from the measured data value for the altitude path-loss modeling. We use to curve fitting method these samples to the well-known log-distance path-loss model in (13). The loss value according to the altitude was analyzed according to the distance. The analysis results confirmed that the measured data at 10 m (fixed) contained all measured data at 20–70 m (step: 10 m). Thus, the path-loss model equation was derived.

5.1. DESST Drone Type. As per measurement scenario 1, dedicated drone and general Wi-Fi signals were simultaneously measured. The DESST signal was identified by applying cross-correlation and the SVD algorithm described in Section 4. Figure 16 shows that the fixed Wi-Fi signal had the same power value. The power value of the DESST signal decreased with time and distance. When SVD and cross-correlation were applied, the general Wi-Fi signal was removed, as shown in Figure 17.

The path-loss modeling for drones was derived by fitting the measured data and classifying them according to distance and altitude. First, the measured data at the distance of 0–70 m (altitude: 0 m) were fitted as follows:

$$PL(d) = L_0 + 10n\log_{10}\frac{d}{d_{ref}} \tag{13}$$

where L_0 is the initial value of the path loss and n expresses the path loss as a scalar value. The distance was 0–70 m, and the reference distance was 5 m and 2m. Table 5 summarizes the details of the model parameters. As shown in Figure 18, the measured power value decreased due to path loss as the drone moved. Figure 19 shows the fitting results according to altitude.

At all measurement points, the loss due to altitude (20–60 m) when included only in the altitude-dependent loss was included in the measured data at 10 m (minimum distance).

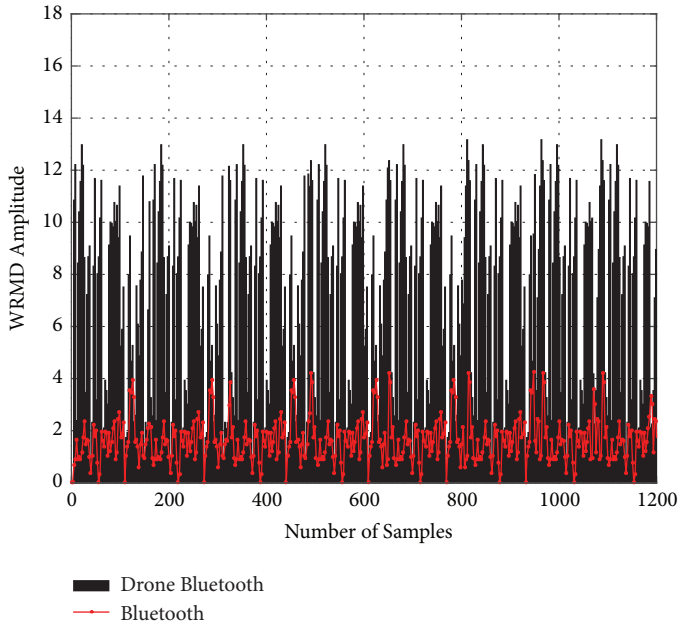

Figure 13: WRMD amplitude of the Bluetooth drone and general signals.

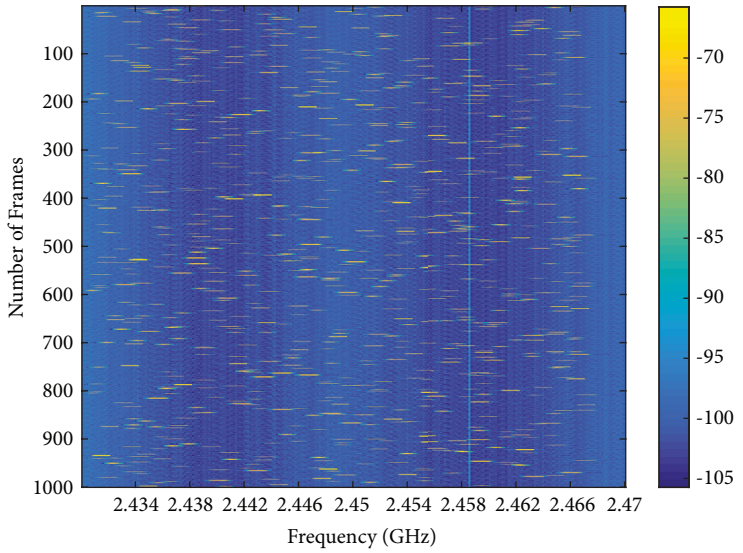

Figure 14: Spectrogram of the Bluetooth signal **before** the WRMD scheme was applied.

Thus, modeling according to altitude is expressed by the measured data at the altitude of 10 m. The loss modeling according to altitude was derived by subtracting the value of −79.97 dB from the data measured at 10 m. The altitude was measured from 0° to 84°, but values above 55° were identified as noise and removed. Therefore, the model according to the altitude was derived from 0° to 55° and is given by

$$PL(\theta) = A(\theta - \theta_0)\exp\left(-\frac{\theta - \theta_0}{B}\right) \quad (14)$$

where A is the path-loss scalar value, the slope is from 0° to 55°, and θ_0 is the angle offset, which is the change in loss with the angle. B is a scalar value for the altitude angle that was set to 103.78°. Table 5 summarizes the details of the model parameters. As shown in Figure 19, the loss due to altitude increased with the path loss of the drone. The model according to altitude derives the loss variation according to the path-loss scalar value and exponential function form.

5.2. Wi-Fi Drone Type. The Wi-Fi drone signal was modeled according to measurement scenarios 1, 2 and identified by I/Q phase analysis. Figures 20 and 21 show the data before and after identification. The fixed general Wi-Fi signal had no change in the power value, and the drone Wi-Fi signal exhibited power attenuation according to the distance.

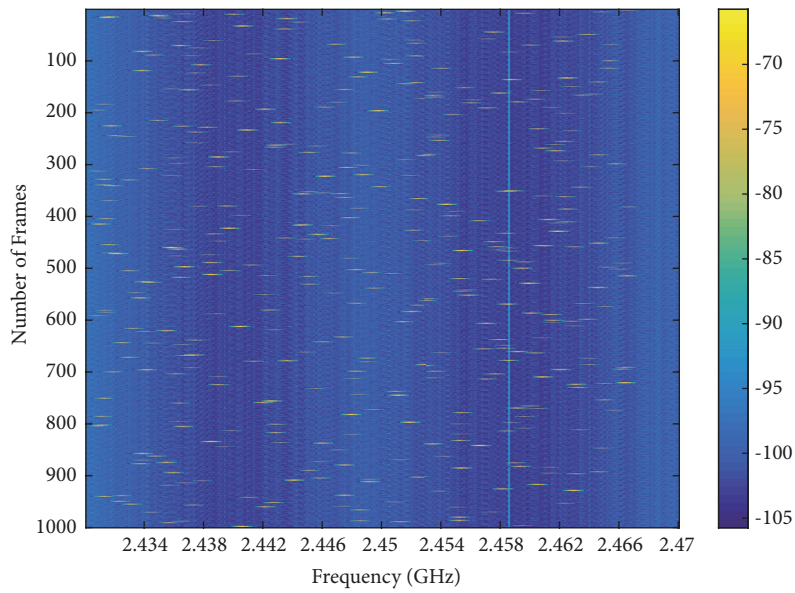

Figure 15: Spectrogram of the Bluetooth signal **after** the WRMD scheme was applied.

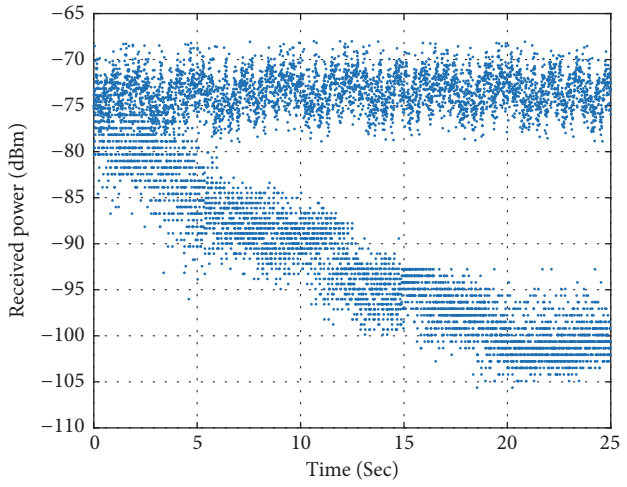

Figure 16: Received power of the DESST drone and general Wi-Fi signal **before** cross-correlation and the SVD scheme were applied.

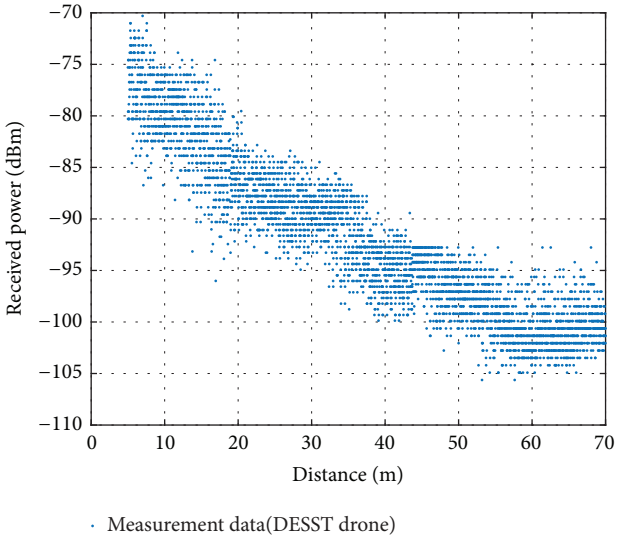

Figure 17: Received power of the DESST drone signal **after** cross-correlation and the SVD scheme were applied.

The distance and altitude modeling were performed in the same way as for the DESST drone. Because the Wi-Fi signal uses a fixed channel, the number of samples was larger than that for the hopping DESST protocol. Modeling was performed only to 55°, which showed the same loss value in modeling according to altitude.

Figures 22 and 23 show the fitting results for the horizontal distance and altitude, respectively. Like the DESST drone, these were modeled by using (13) and (14). The Wi-Fi drone model looks similar to the DESST drone model but includes frequency attenuation because of the use of a constant channel. The Wi-Fi drone modeling also explains the interference on DESST frequency hopping.

5.3. Bluetooth Drone Type. Propagation modeling for communication equipment using other communication standards is an important factor in cell design. The drones using Bluetooth, which is an ISM communication method, were modeled according to measurement scenario 4. The Bluetooth drones were measured up to a horizontal distance and altitude of 20 m. Figures 24 and 25 show the results before and after the WRMD scheme was applied. We confirmed that the number of signal samples was small because the Bluetooth signal also hopped. The drone Bluetooth signal was identified by the WRMD algorithm. Despite the small flying distance, the signal showed a great deal of power attenuation.

Table 5: Model parameters.

Parameters	Symbol	DESST drone	Wi-Fi drone	Bluetooth drone
Path-loss initial value	L_0	−71.41	−77.16	−72.91
Path-loss scalar	n	2.558	2.275	2.275
Distance	d	5-70 m	5-70 m	3-20 m
Reference distance	d_{ref}	5 m	5 m	2 m
Excess path-loss scalar	A	1.269	1.152	0.755
Angle	θ	0-55°	0-55°	0-28.84°
Angle offset	θ_0	6.577	6.027	−2.022
Angle scalar	B	89.59	93.15	56.8
Std. mean	μ	−1.57	−2.69	0.07
Std. variance	σ	8.01	8.85	3.02
Frequency band		2.4005~2.4925 GHz	2.402~2.494 GHz	2.402~2.480 GHz

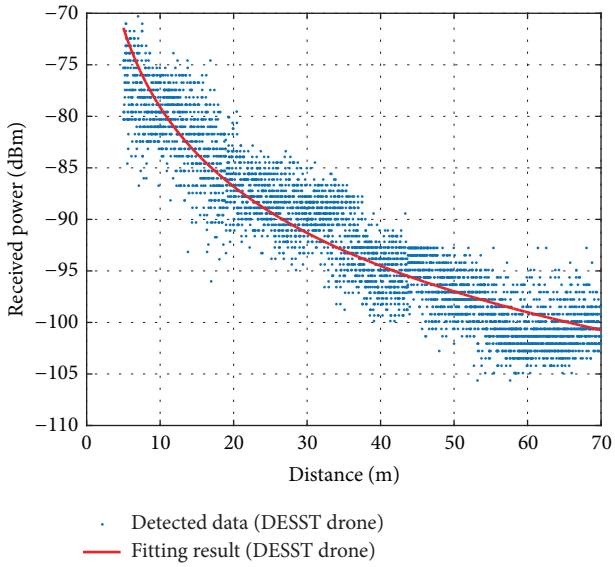

Figure 18: Fitting results for DESST drones according to the horizontal distance.

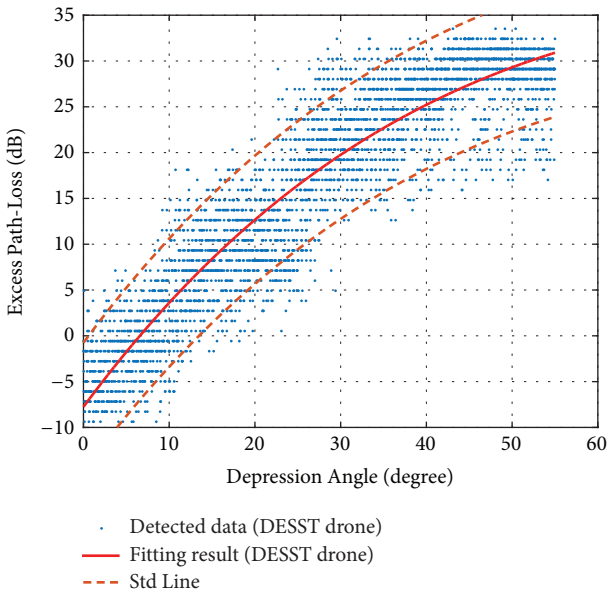

Figure 19: Fitting results for DESST drones according to the depressing angle.

Figures 26 and 27 show the fitting results for the horizontal distance and altitude, respectively. The maximum modeled depression angle was 28.84°. Equations (13) and (14) were also used for the model to compare the three communication methods. The fitting results include the down-tilt of the antenna pattern attenuation of the Bluetooth signal.

5.4. Final Proposed Path-Loss Model. We propose a model for the horizontal distance and altitude to identify the signal of three types of drones. Before the measurements, we confirmed the Federal Communications Commission (FCC) certification documents to calculate the power budget. The transmit power of the DESST drone type is -22.14 dBm, that of the Wi-Fi drone type is -23 dBm, and that of the Bluetooth drone type is -29.71 dBm. The transmit antenna gain of each drone is 3.9 dBi, 2.5 dBi, and -0.6 dBi, respectively [22–24]. As a result of calculating the Free-Space Path Loss and receive antenna gain 3 dBi, the expected receive power of each drone is -69.26 dBm, -71.52 dBm, and -76.77 dBm, respectively. This model includes fading for the distance and altitude and propagation attenuation for shadowing. As a result, the initial receive power of each drone was measured as -71.41 dBm, -77.16 dBm, and -72.91 dBm, respectively. Figures 28 and 29 show the model according to the horizontal distance and altitude.

The proposed model equation is as follows:

$$PL_{drone}(d,\theta) = L_0 + 10n\log_{10}\frac{d}{d_{ref}} + A(\theta-\theta_0)\exp\left(-\frac{\theta-\theta_0}{B}\right) + N(\mu,\sigma) \quad (15)$$

where L_0 is the initial path loss and n is expressed by the scalar value of the path loss. The distance is 0–70 m, and the reference distance is 5 m. A is the scalar value

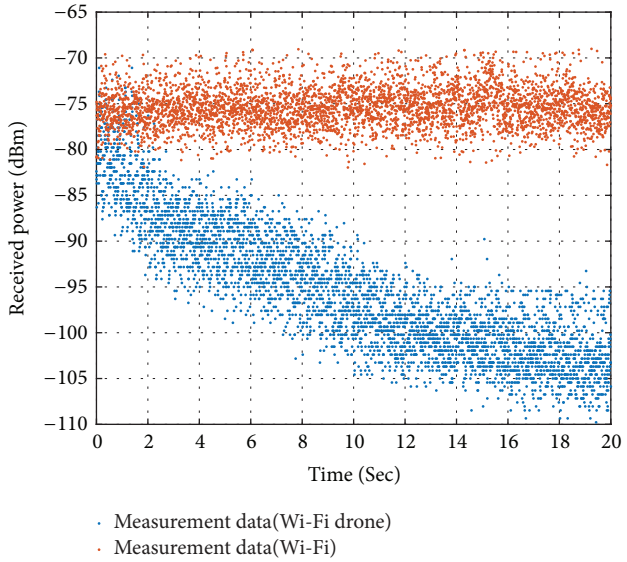

Figure 20: Received power of the general Wi-Fi and drone Wi-Fi signal **before** the I/Q phase scheme was applied.

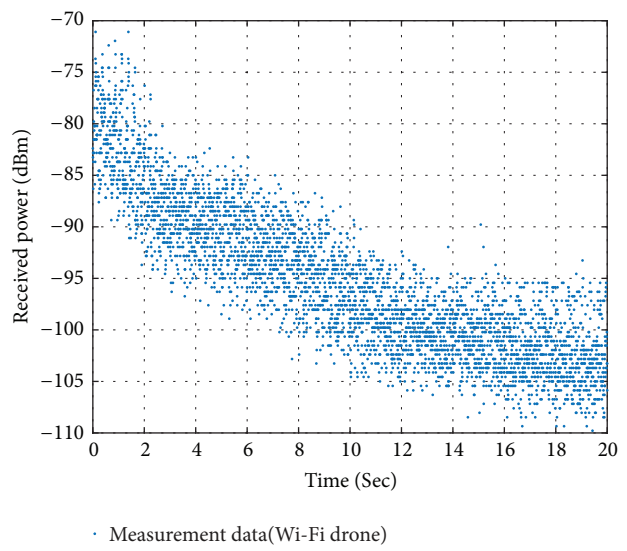

Figure 21: Received power of the drone Wi-Fi signal **after** the I/Q phase scheme was applied.

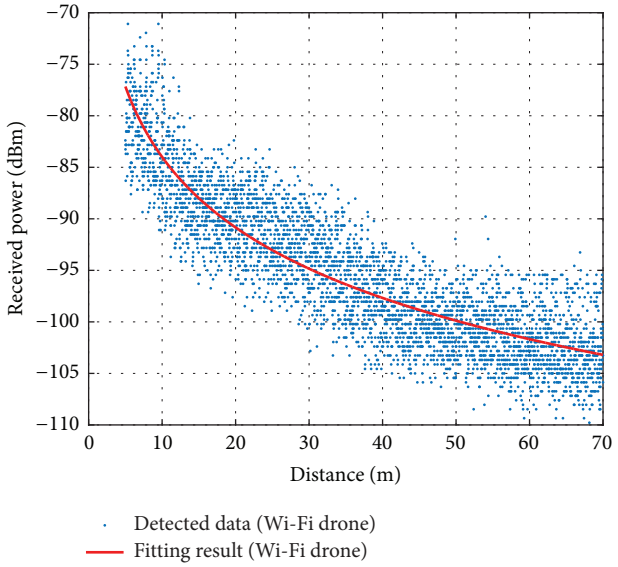

Figure 22: Fitting results for the Wi-Fi drones according to the horizontal distance.

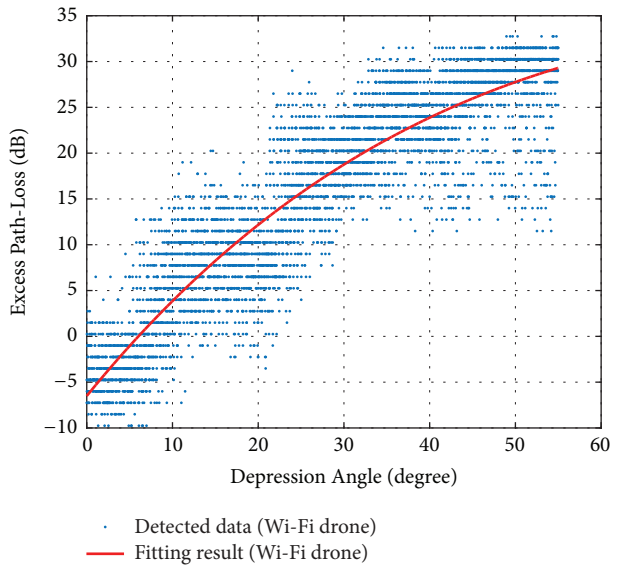

Figure 23: Fitting results for the Wi-Fi drones according to the depressing angle.

of the path loss, and the slope is 0°–55°. θ_0 is the angle offset, which is the change in the loss with the angle. B is the scalar value of the altitude angle. The proposed model equation depends on the fitting line and cannot represent all received data. Therefore, the variation in the actual measured data is represented by a probability distribution function. N represents a normal probability distribution, μ is the mean value, and σ is the variance. Table 5 summarizes the details of the model parameters. Our model shows the power attenuation of drones in the ISM band environment.

The results showed that our proposed model for the new aerial terrestrial cellular system at the ISM band frequency predicts the drone movement appropriately. The method can calculate the propagation characteristics according to whether the drone is moving horizontally or vertically. The propagation characteristics can be predicted for specific drones in contrast to widely existing propagation models.

6. Verification of the Proposed Model

To verify the validity of the measurement results, we configured a real propagation environment in a ray-tracing simulation tool. The simulation environment consists of buildings and forest information similar to a real environment. The simulation tool, EIR Tracer, is provided by ETRI (Electronics and Telecommunications Research Institute). The ray-tracing

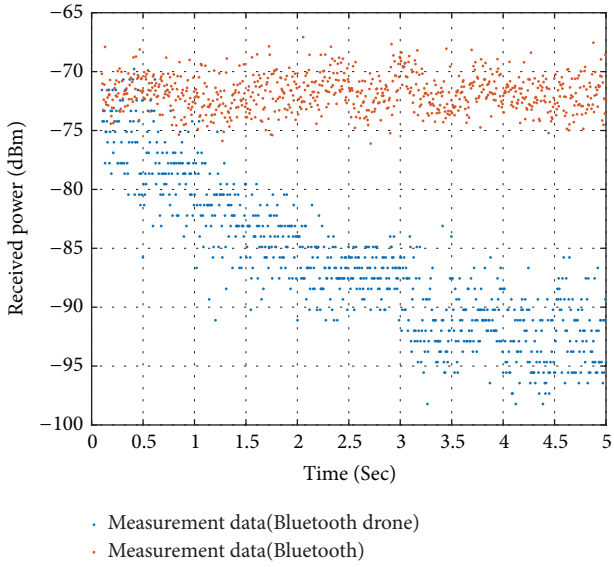

Figure 24: Received power of the general Bluetooth and drone Bluetooth signals **before** the WRMD scheme was applied.

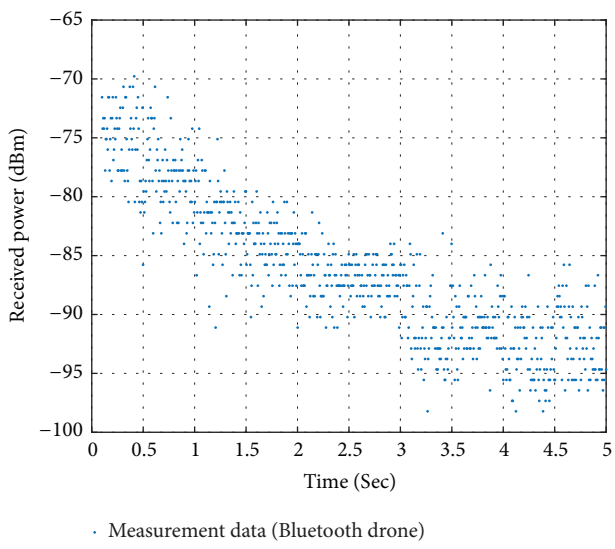

Figure 25: Received power of the drone Bluetooth signal **after** the WRMD scheme was applied.

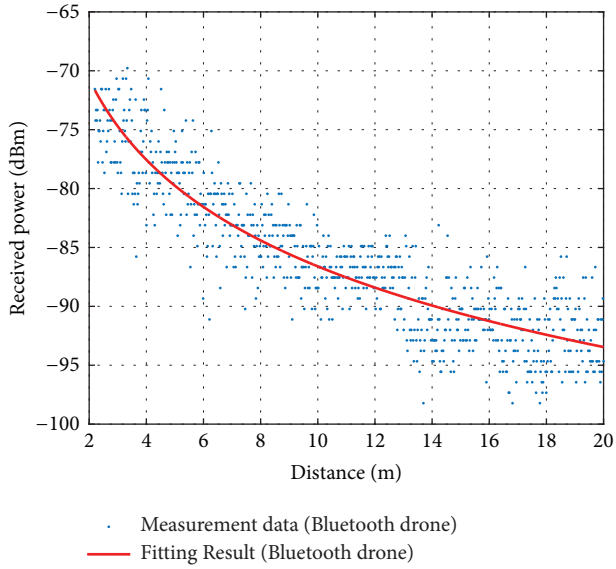

Figure 26: Fitting results for the Bluetooth drones according to the horizontal distance.

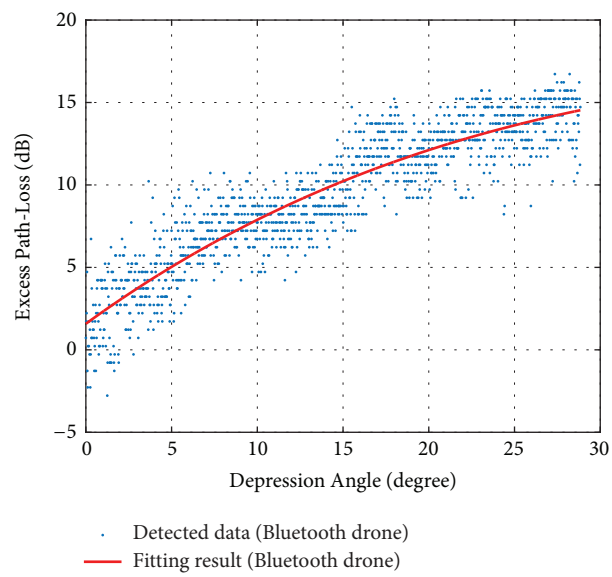

Figure 27: Fitting results for the Bluetooth drones according to the depressing angle.

simulation is composed of three measurement environments and two scenarios and is compared with the proposed model for distance d through averages of received power. Figures 30–32 present the ray-tracing simulation screen at different distances and altitudes, respectively. The Wi-Fi and DESST models were compared with the 802.11b standard model, and the Bluetooth model was compared with the 802.15.1 standard model [25–28]. Figures 33 and 34 show the ray-tracing simulation results of each standard model and the proposed model. The ray-tracing results are slightly different from our proposed model, but their tendencies are similar, with a difference of within 5 dB. Therefore, the proposed model in this paper is reliable.

7. Conclusion

For 5G aerial networks, detecting the movement of various drones is affected by the radio propagation characteristics. Therefore, detecting the drone RF signal and predicting the propagation characteristics are an essential part of designing a 5G aerial communication system. In this study, we focused on the RF detection of various drones and analysis of the propagation characteristics at the ISM band frequency. We considered three drones with different communication modes at Chungbuk National University. The measured data were identified according to the proposed identification algorithm for different measurement scenarios. We identified

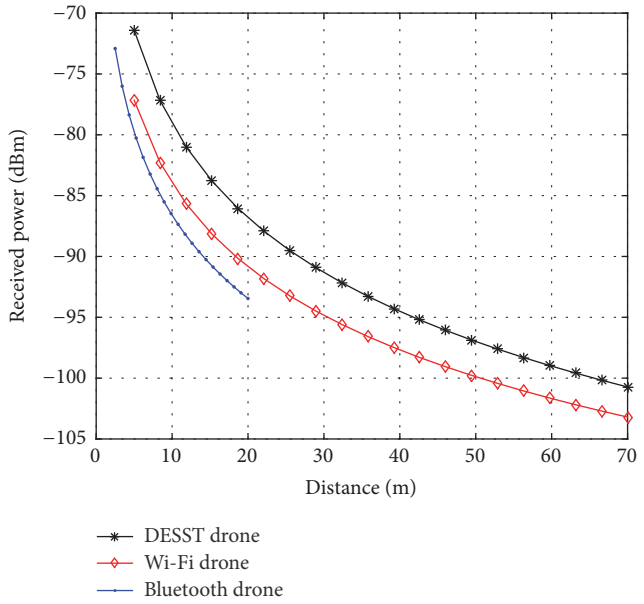

Figure 28: Proposed models for the three drones according to the horizontal distance.

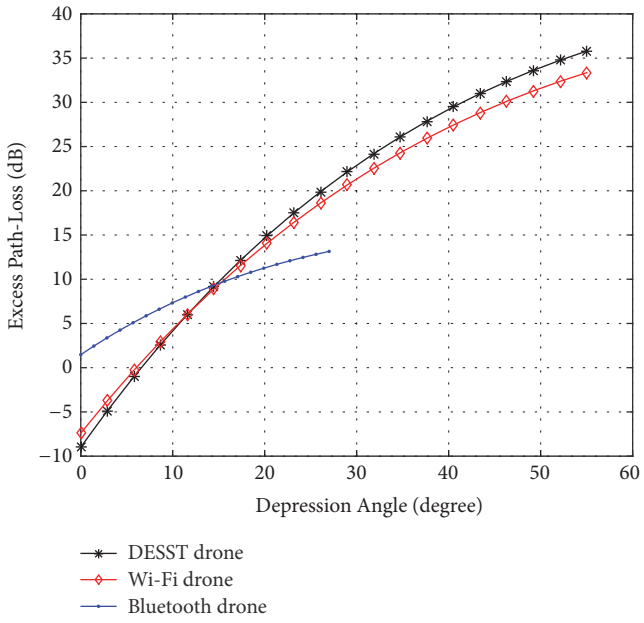

Figure 29: Proposed models for the three drones according to the depressing angle.

DESST protocol, Wi-Fi, and Bluetooth signals. The results confirmed that the algorithm can identify the RF characteristics of each drone. We propose a propagation attenuation equation for identifying signals up to a horizontal distance of 70 m and altitude angle of 55°. To verify the validity of the measurement results, we created simulated conditions based on a GIS map in a real environment. The simulated environment consists of buildings and forest information similar to a real environment at Chungbuk National University in Korea. The results showed that our proposed model for a new

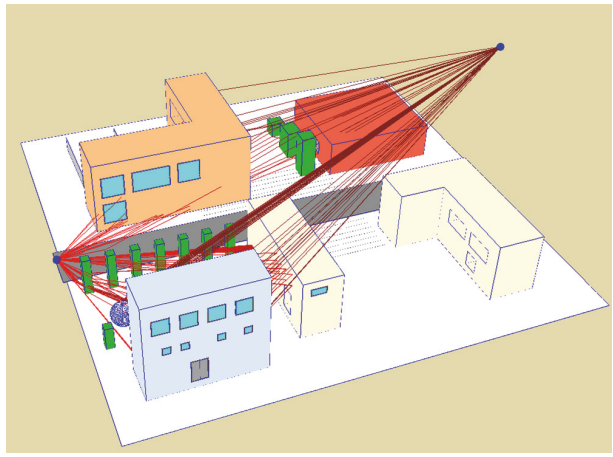

Figure 30: Ray-tracing simulation screen (site 1, d: 70 m, altitude: 20 m).

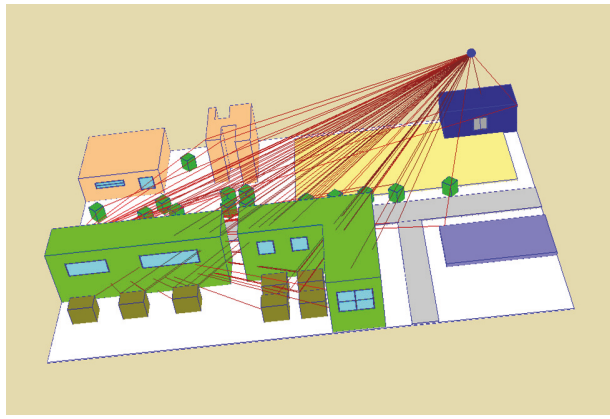

Figure 31: Ray-tracing simulation screen (site 2, d: 50 m, altitude: 30 m).

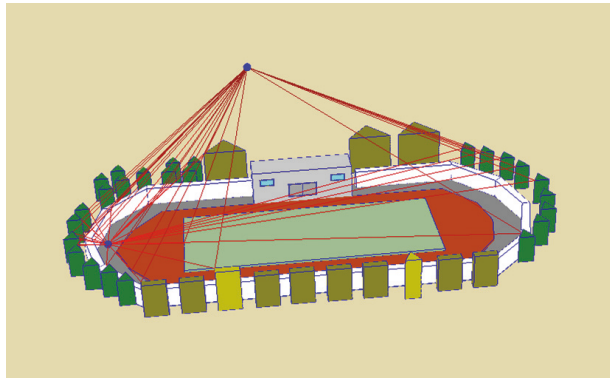

Figure 32: Ray-tracing simulation screen (site 3, d: 30 m, altitude: 50 m).

aerial communications system in the ISM band appropriately predicted the signal according to the drone movement. The proposed model is presented in consideration of the most widely used drones in Korea, but it is not applicable to all drones and can be applied only to measured drones and scenarios.

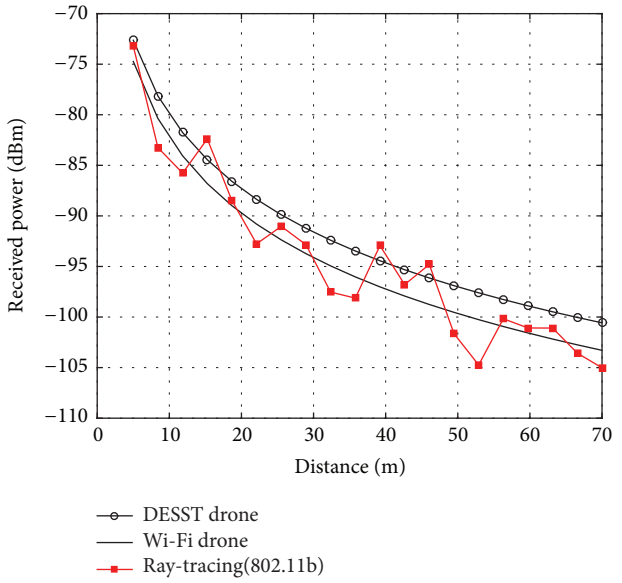

FIGURE 33: Comparison of the proposed model with the ray-tracing result (802.11b standard and proposed model).

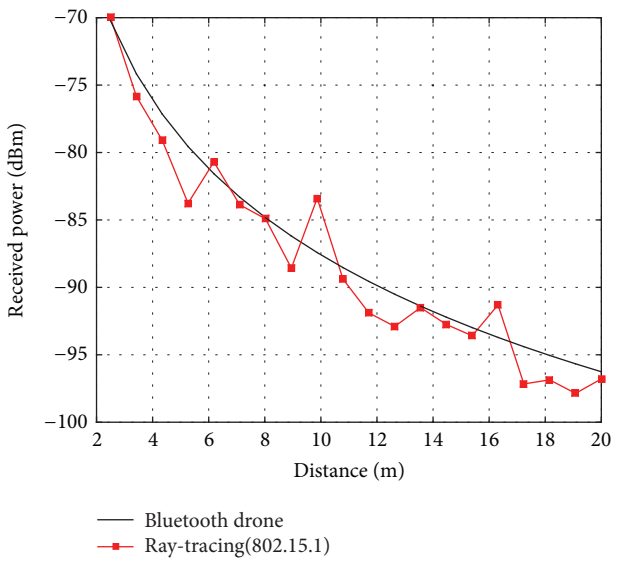

FIGURE 34: Comparison of the proposed model with the ray-tracing result (802.15.1 standard and proposed model).

Data Availability

The data used to support the findings of this study are available from the corresponding author upon request.

Conflicts of Interest

The authors declare that they have no conflicts of interest.

Acknowledgments

This work was supported by the ETRI (Electronics and Telecommunications Research Institute) affiliated research institute and the National Security Research Institute.

References

[1] A. Al-Hourani and K. Gomez, "Modeling Cellular-to-UAV Path-Loss for Suburban Environments," *IEEE Wireless Communications Letters*, vol. 7, no. 1, pp. 82–85, 2018.

[2] A. Al-Hourani, "Coverage and rate analysis of aerial base stations [Letter]," *IEEE Transactions on Aerospace and Electronic Systems*, vol. 52, no. 6, pp. 3077–3081, 2016.

[3] "ITU: World Radiocommunication Conference 2015(WRC-15)," Council Resolution 528.

[4] H3GPP TSG RAN WG1, R1-1704429, R1-1704430, and R1-1704431, "Drone Connectivity, Interference and Channel Models," 2017.

[5] R. Amorim, H. Nguyen, P. Mogensen, I. Z. Kovács, J. Wigard, and T. B. Sørensen, "Radio channel modeling for UAV communication over cellular networks," *IEEE Wireless Communications Letters*, vol. 6, no. 4, pp. 514–517, 2017.

[6] M. Simunek, F. P. Fontán, and P. Pechac, "The UAV low elevation propagation channel in urban areas: Statistical analysis and time-series generator," *IEEE Transactions on Antennas and Propagation*, vol. 61, no. 7, pp. 3850–3858, 2013.

[7] M. Simunek, P. Pechac, and F. P. Fontan, "Excess loss model for low elevation links in urban areas for UAVs," *Radioengineering*, vol. 20, no. 3, pp. 561-560, 2011.

[8] M. Simunek, F. P. Fontan, P. Pechac, and F. J. D. Otero, "Space diversity gain in urban area low elevation links for surveillance applications," *IEEE Transactions on Antennas and Propagation*, vol. 61, no. 12, pp. 6255–6260, 2013.

[9] M. Simunek, P. Pechac, and F. P. Fontan, "Feasibility of UAV link space diversity in wooded areas," *International Journal of Antennas and Propagation*, vol. 2013, Article ID 890629, 5 pages, 2013.

[10] N. Goddemeier and C. Wietfeld, "Investigation of air-to-air channel characteristics and a UAV specific extension to the rice model," in *Proceedings of the IEEE Globecom Workshops, GC Wkshps 2015*, pp. 1–5, San Diego, Cal, USA, December 2015.

[11] H. T. Kung, C. Lin, T. Lin, S. J. Tarsa, and D. Vlah, "Measuring diversity on a low-altitude UAV in a ground-to-air wireless 802.11 mesh network," in *Proceedings of the IEEE Globecom Workshops (GC'10)*, pp. 1799–1804, Miami, Fla, USA, December 2010.

[12] X. Cai, A. Gonzalez-Plaza, D. Alonso et al., "Low altitude UAV propagation channel modelling," in *Proceedings of the 11th European Conference on Antennas and Propagation, EUCAP 2017*, pp. 1443–1447, France, March 2017.

[13] R. M. Gutierrez, H. Yu, Y. Rong, and D. W. Bliss, "Time and frequency dispersion characteristics of the UAS wireless channel in residential and mountainous desert terrains," in *Proceedings of the 14th IEEE Annual Consumer Communications and Networking Conference, CCNC 2017*, pp. 516–521, USA, January 2017.

[14] Recommendation ITU-R M.2531, "WINNER II Channel Models," 2007.

[15] N. Czink and C. Oestges, "The COST 273 MIMO channel model: three kinds of clusters," in *Proceedings of the 2008 IEEE 10th International Symposium on Spread Spectrum Techniques and Applications (ISSSTA)*, pp. 282–286, Bologna, August 2008.

[16] Recommendation ITU-R P. 1411-5, "Propagation and Prediction Methods for the Planning of Short-Range Outdoor Radio Communication System," 2009.

[17] Recommendation ITU-R P.1407-4, "Multipath propagation and parameterization of its characteristics," 2009.

[18] https://www.droneii.com/top20-drone-company-ranking-q3-2016.

[19] C. F. Chiasserini and R. R. Rao, "Coexistence mechanisms for interference mitigation between IEEE 802.11 WLANs and Bluetooth," in *Proceedings of the IEEE Infocom 2002*, pp. 590–598, USA, June 2002.

[20] Recommendation ITU-R SM.1600-2, "Technical identification of digital signals," 2015.

[21] F. Soldovieri and G. Gennarelli, "Exploitation of ubiquitous Wi-Fi devices as building blocks for improvised motion detection systems," *Sensors*, vol. 16, no. 3, 2016.

[22] Federal Communications Commission(FCC) RDG160806002-00C, "Mavic Pro Test Report," 2016.

[23] Federal Communications Commission(FCC) DM124239, "WiFi Camera Drone Test Report," 2016.

[24] Federal Communications Commission(FCC) RR051-14-106526-2-A Ed.0, "Quadricopter controlled by smartphones Test Report PARROT," 2015.

[25] T. Chrysikos and S. Kotsopoulos, "Site-specific Validation of Path Loss Models and Large-scale Fading Characterization for a Complex Urban Propagation Topology at 2.4 GHz," in *Proceedings of the International Multi Conference of Engineers and Computer Scientists*, 2013.

[26] D. Plets, R. Mangelschots, K. Vanhecke, L. Martens, and W. Joseph, "A mobile app for real-time testing of path-loss models and optimization of network planning," in *Proceedings of the 27th IEEE Annual International Symposium on Personal, Indoor, and Mobile Radio Communications, PIMRC 2016*, Spain, September 2016.

[27] Recommendation ITU-R P. 1238-7, "Propagation Data and Prediction Methods for the Planning of Indoor Radio Communication Systems and the Radio Local Area Networks in the Frequency Range 900 MHz to 100 GHz," 2001.

[28] S. Kubal, K. Staniec, and R. J. Zieliński, "Analysis of the radiowave propagation in an underground mine based on the modified Ray launching method," *IET Microwaves, Antennas & Propagation*, vol. 9, no. 12, pp. 1241–1248, 2015.